IHJPAS. 37 (2) 2024
Ibn Al-Haitham Journal for Pure and Applied Sciences
Journal homepage: jih.uobaghdad.edu.iq
PISSN: 1609-4042, EISSN: 2521-3407

A Study of the Relationship between the Two Types of Crystallite Dislocation Density and the Particle Size of Barium Oxide (BaO) Nanoparticle

Shefaa S. Abdul-Jabbar[1*] and Khalid H. Harbi[2]
[1,2] Department of Physics, College of Education for Sciences (Ibn-AL-Haitham), University of Baghdad, Baghdad, Iraq.
*Corresponding Author.

Received: 10 April 2023 Accepted: 25 June 2023 Published: 20 April 2024
doi.org/10.30526/37.2.3393

Abstract

The research is demonstrating the use of X-ray diffraction pattern obtained experimentally from barium oxide powder. The X-ray diffraction pattern of the barium oxide nanoparticle sample was analyzed through the program to obtain the mean intensity width values and use these values to extract the particle size for all diffraction pattern lines using the Scherrer method. The nanoparticle size was calculated for each barium oxide line. Then the dislocation density was calculated through two mathematical equations, one of which depended on the particle size and the other depended on the integral breadth, a comparison was made between the results of the two dislocation densities and the particle size, where it was found that the dislocation density is inversely proportional to the particle size for both types, but the values of the dislocation density depend on the strain the retina will be bigger. Also, the relationship between the values of unit cell number and particle size was studied.

Keywords: BaO, XRD, two type Dislocation density, Scherrer equation.

1. Introduction

The X-ray diffraction method was first used to determine the ideal composition of a material, and Von Laue made the first discovery of X-ray diffraction in 1912 when he found that the incident rays from a crystal might be diffracted by the surroundings, in the years that followed, this technique has been widely used in scientific and applied fields [1-3]. A practical way for figuring out the average size of nanocrystallites in bulk nanocrystalline materials is x-ray diffraction, the scientist, Paul Scherer, presented his results in 1918 and included an equation in the name of Scherrer [4]. X-ray diffraction is an accurate method for detecting the size of crystals in nanoparticles, noting that the size of the crystals is not equal to the size of the particle particles [5-7]. The dependence of X-ray line analysis on the diffraction angle (Bragg's angle in the diffraction) makes it necessary to rely on accurate methods in analyzing the integrated width of each line of the X-ray diffraction lines, regardless of the methods used in the analysis [8-12]. In addition to the Scherrer method, another method was used to calculate particle size as well as lattice strain, and other physical parameters were extracted, such as strain values for X-ray reflection peak lines, dislocation density, and unit cells, also the particle size can be used to calculate the dislocation density of materials [13-18].

2. Theory

2.1. Scherrer method

The profile of the diffraction line, it possible to determine the crystal size, strain, crystal defects, and crystalline persistence deviation in imperfect crystals, and the crystal size value can be calculated by applying the Scherrer equation [19-22].

$$D = (k\lambda / FWHM) \cos \theta \quad (1)$$

Where (k) is the shape constant and is equal to (0.89), (θ) is the diffraction angle of Bragg, (λ) is the wavelength of the X-ray and is equal to (0.15406 nm), (D) is the crystallite size and (FWHM) is full width at half maximum integral breadth (β)

$$\varepsilon=\beta \cot \theta/4 \quad (2)$$

$$\varepsilon=\beta/4 \tan \theta \quad (3)$$

Where parameter (β) represents (integral breadth), and parameter (ε) is representing (lattice strain) [23,24].

Also, the dislocation density can be calculated through the following relationship:

$$\delta= 1/ D^2 \quad (4)$$

Where δ is the dislocation density of the material and D^2 crystallite size square. The defect occurring in the crystal structure system strongly affects the properties of the material. The number of dislocation lines per unit crystal volume is called the dislocation density and can be calculated from the following equation [25-27]:

$$\delta=15 \beta_{hkl} \cos\theta / 4aD \quad (5)$$

Where (a) is lattice constant it is estimated by unit (Å), (β_{hkl}) is intensity breadth for each peak, (θ) is the angle of diffraction (Bragg angle). And then used equation (6) to calculate the number of unit cell which equal to: [28,29]

$$n = \pi (4/3) \text{ x } (D/2)^3 \text{x } (1/V) \quad (6)$$

Where V is the cell volume.

3. Laboratory Tests

The powder of BaO nanoparticle is screened for comprehensive diagnostics as described below. Using a Japanese SHIMADZU model (6000) Cu-k radiation diffractometer with a wavelength of 1.5406 Å, a powder XRD pattern was obtained. The operating voltage and filament current were both set at 30 mA and 40 kV, respectively. **Figure 1,** shows the XRD pattern of the powdered barium oxide nanoparticles. The structure of raw BaO is tetragonal reflected in all peaks in the diffraction pattern. This diffraction model was used to calculate the total area of the X-ray diffraction lines.

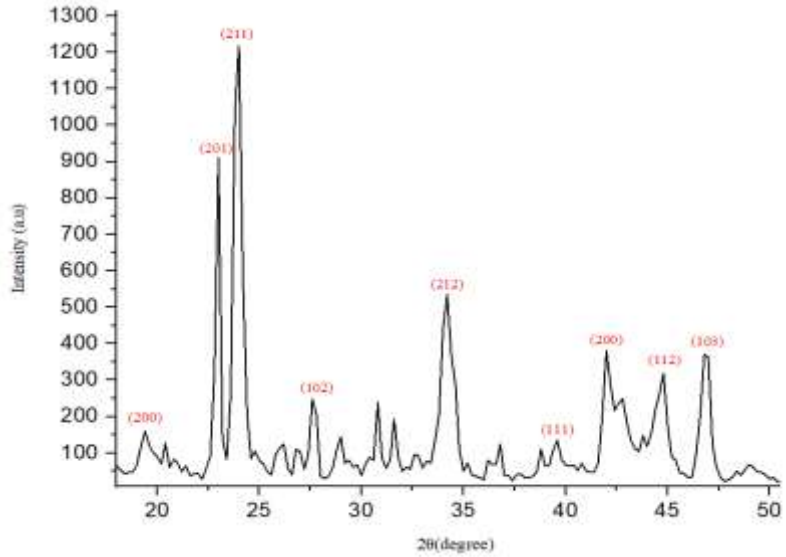

Figure 1. XRD pattern of BaO nanoparticles

Through the (XRD) patterns shown in **Figure 1,** the limits of the angles of the XRD pattern are from 20 to 80. It was extracted from SHIMADZU and shows sample BaO nanoparticles to all profile lines five peaks at 2θ = 19.56°, 23. 99 °,27.68 °,34.23 °, 39.58°, 44.62°, and 46.85° could be indexed at (200), (201), (102), (212),(111), (112), and (103) planes of the tetragonal phase BaO which matches the standard JCPDS card no.26-0178 [30].In this study, we have used Origin Pro software to calculate the area under the curve and the height of the line profile then used the equation $\beta = A/I_o$ to find the Integral Breadth (I_B). In addition; (β_{hkl})radianthe results are listed in **Table 1**.

4. Results and discussions

In the Scherrer method, Through the profile of the lines of the XRD patterns of the barium oxide nano powder, the graph of the values of each of the peak (I_o)intensity and the angle of diffraction (2θ) was determined by applying a program to convert the digital data into a graph to draw each peak of the barium oxide pattern, which was carried out by the application of the Origin Pro program, each peak in the model was then fit to access the line clear of peaks. After fitting all peaks, 40 steps were added to the composition of the lines for each peak to obtain a clear and prominent line with more accuracy, and the area under the curve was estimated after intensity subtraction to obtain the removal of background values for each peak. Then, the integral breadth for each peak was calculated from the equation $\beta = A/I_o$ [28] where (A) represents the area under the curve for each peak and (I_o)is the magnitude of the intensity for each peak. The shape of the peaks curve was determined, as shown in **Figure 2**.

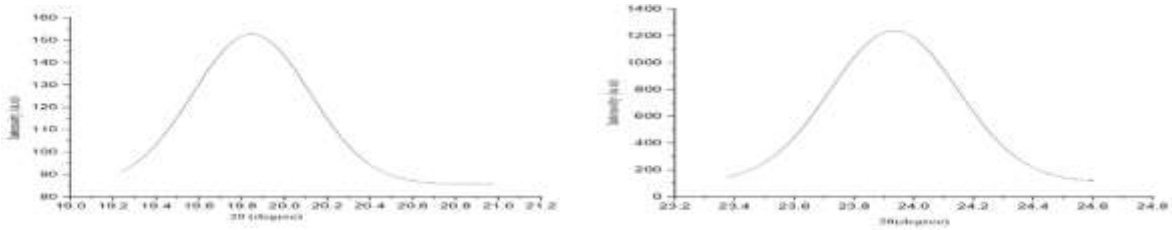

(A)After fitting of peak (200) (B)After fitting of peak (201)

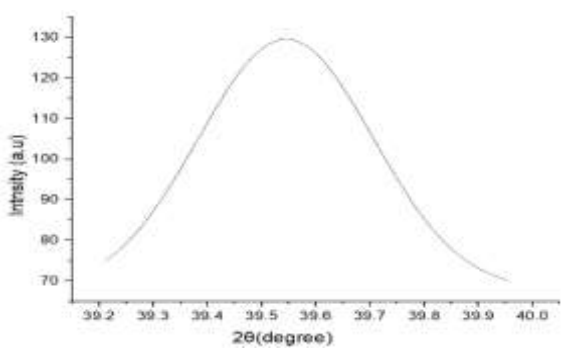

(C)After fitting of peak (102)

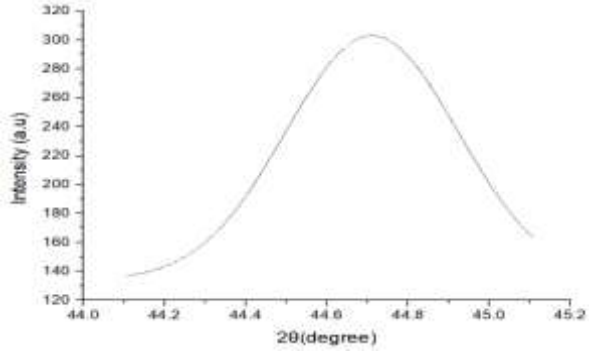

(D)After fitting of peak (212)

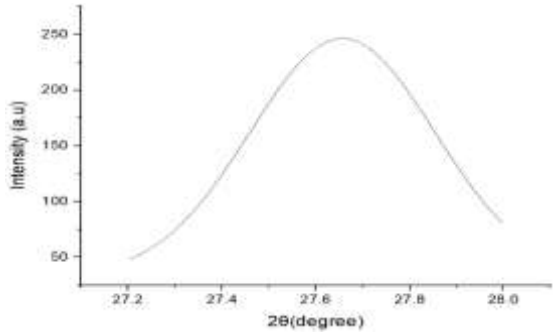

(E)After fitting of peak (111)

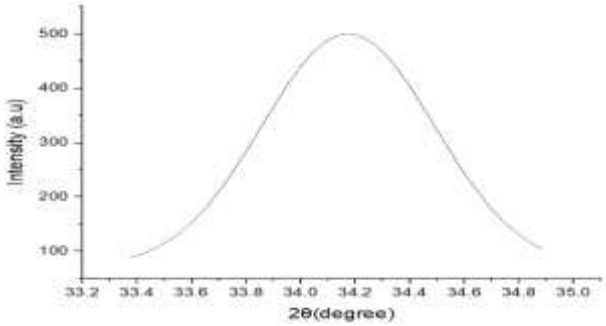

(F) After fitting of peak (112)

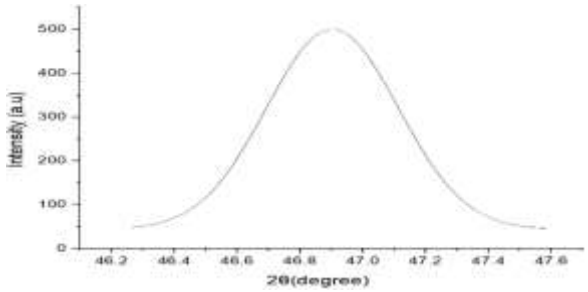

(G)After fitting of peak (103)

Figure 2. (A, B, C, D, E, F, G). After fitting for peak of (BaO) nanoparticles

After that, each curve was divided into 40 steps to include all parts of the curve by calculating the area, and this was done through a program designed to calculate the area under the curve, as shown in **Figure 3**.

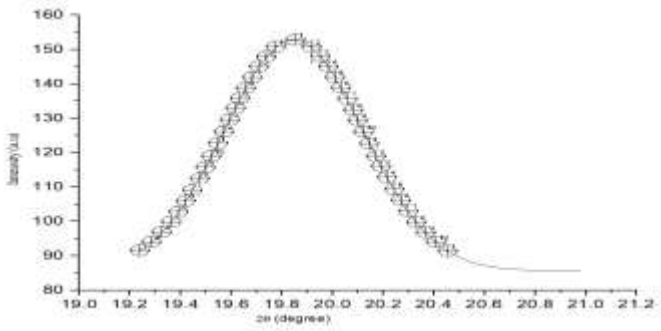

(A)Fitted of peak (200)

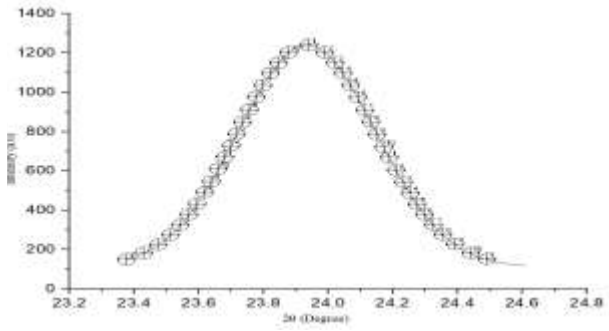

(B)Fitted of peak (201)

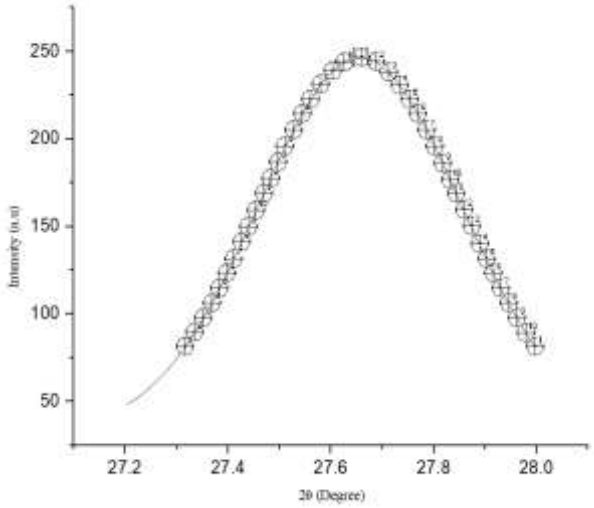

(C) Fitted of peak (102)

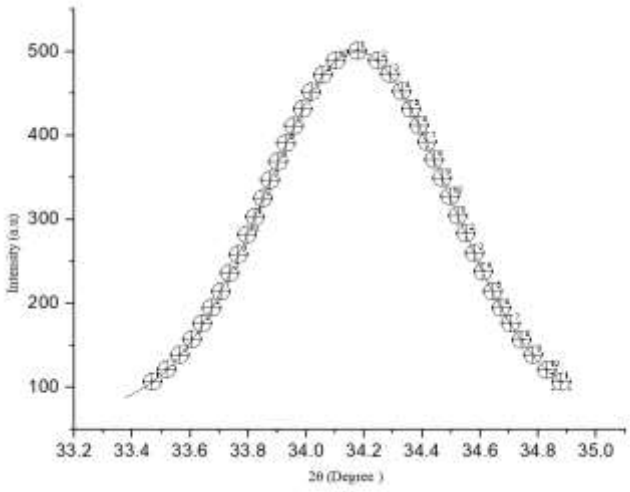

(D) Fitted of peak (212)

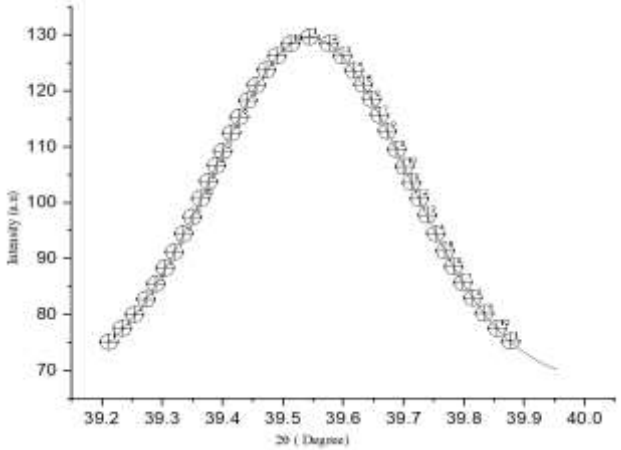

(E)Fitted of peak (111)

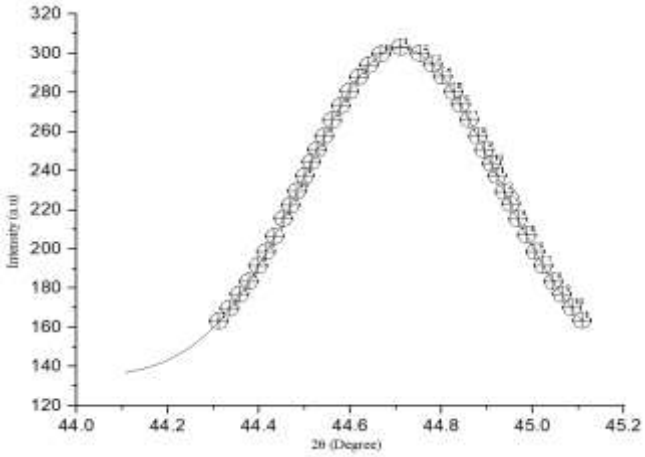

(F)Fitted of peak (112)

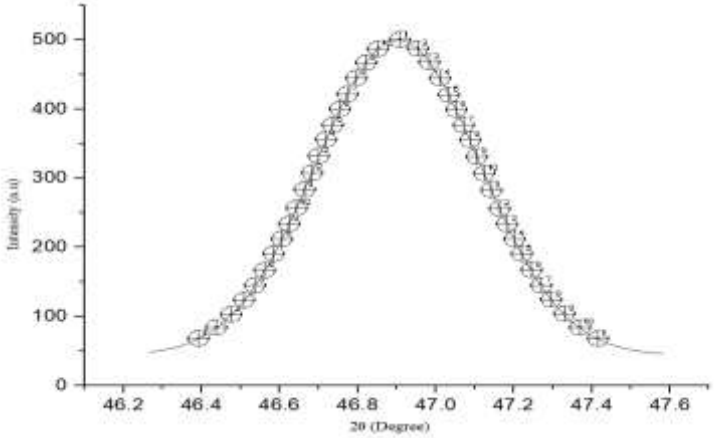

(G)Fitted of peak (103)

Figure 3. (A, B, C, D, E, F, G). Fitting for peak of (BaO) nanoparticles

The results of the area under the curve that was calculated for each curve of **Figure 3.**, were included in **Table 1**, and the (FWHM) and the integral breadth (β_{hkl}).

Table 1. Area under the curve and FWHM and integral breadth (β_{hkl}) to all peaks

(*hkl*)	2θ(degree)	θ	Cosθ	tanθ	FWHM	β_{hkl} (deg)	β(rad)=β(deg)x(3.14/180)
200	19.84666	9.92333	0.98503924	0.17494755	0.6039672	0.6039672	0.010535872
201	23.93418	11.96709	0.97826686	0.21195629	0.4902873	0.4902873	0.00855279
102	27.65708	13.82854	0.97101534	0.24615179	0.3881783	0.3881783	0.006771555
212	34.17333	17.086665	0.95586142	0.30738542	0.6957364	0.6957364	0.012136735
111	39.54458	19.77229	0.94104448	0.35947593	0.3461925	0.3461925	0.006039136
112	44.71053	22.355265	0.92484328	0.41125713	0.4366165	0.4366165	0.007616532
103	46.90382	23.45191	0.91739443	0.43381472	0.475513	0.475513	0.00829506

Through the data extracted in **Table 1,** extract the crystallite size for each peak of the XRD patterns, the dislocation density (δ), size strain (ε), and the unit cell (n) as shown in the **Table 2**.

After extracting the value of the crystalline size and the crystalline dislocation density, the relationship between them was found graphically, where the crystalline size increases with decreases of linear dislocation density, and this relationship is shown in the graph in **Figure 4.**

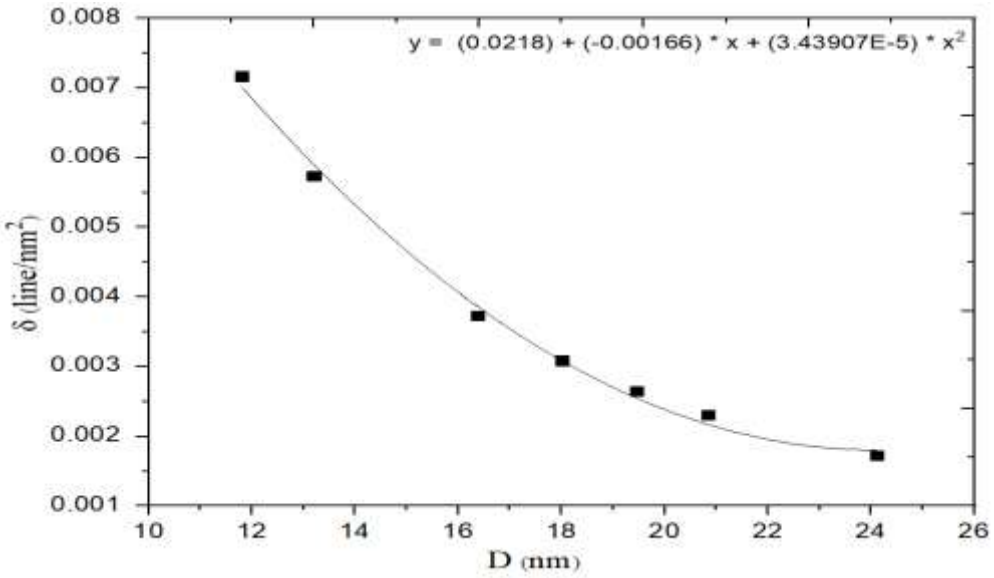

Figure 4. The relationship between dislocation density (δ) and crystalline size (D)

Table 2. The crystallite size value, dislocation density (δ), size strain (ε), and the unit cell (n) for all peaks.

D=K*λ/βcosθ (nm)	δ=1/D² (lin/nm²)	ε=β/4tanθ	n	δ*10^15(Lin/m²)
13.21195693	0.005728827	0.015055759	13488	5.728827
16.38800347	0.00372347	0.010087917	25741	3.72347
20.85339108	0.00229957	0.006877418	53036	2.29957
11.81937121	0.007158322	0.009870942	9657	7.158322
24.12716118	0.001717859	0.004199958	82141	1.717859
19.46550805	0.002639177	0.004630031	43136	2.639177
18.01837157	0.003080129	0.004780301	34213	3.080129

From the extracted data table, the relationship was clarified for both the unit cell and the crystalline dislocation density, as the graph between them showed that as the number of unit cells of the crystalline lattice increases with decreases of linear dislocation density, as shown in the graph of **Figure 5**.

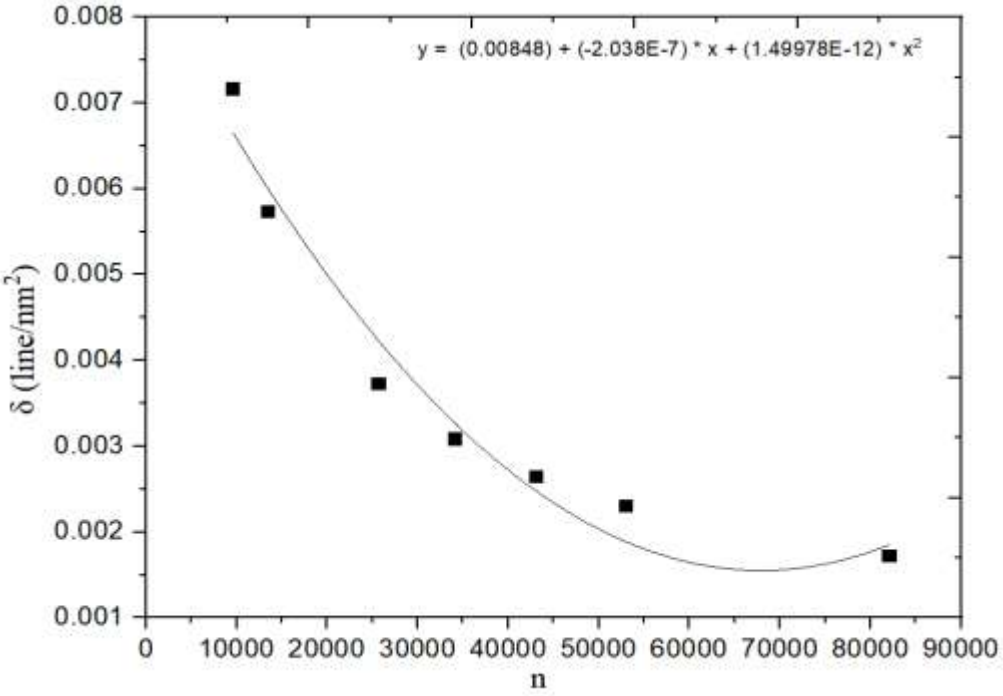

Figure 5. The relationship between dislocation density (δ)and unit cell (n)

The results showed that the relationship between the unit cell and the crystalline size is that the crystalline size increases with increase of number of unit cells for crystalline lattice, as shown in the graph in the **Figure 6**.

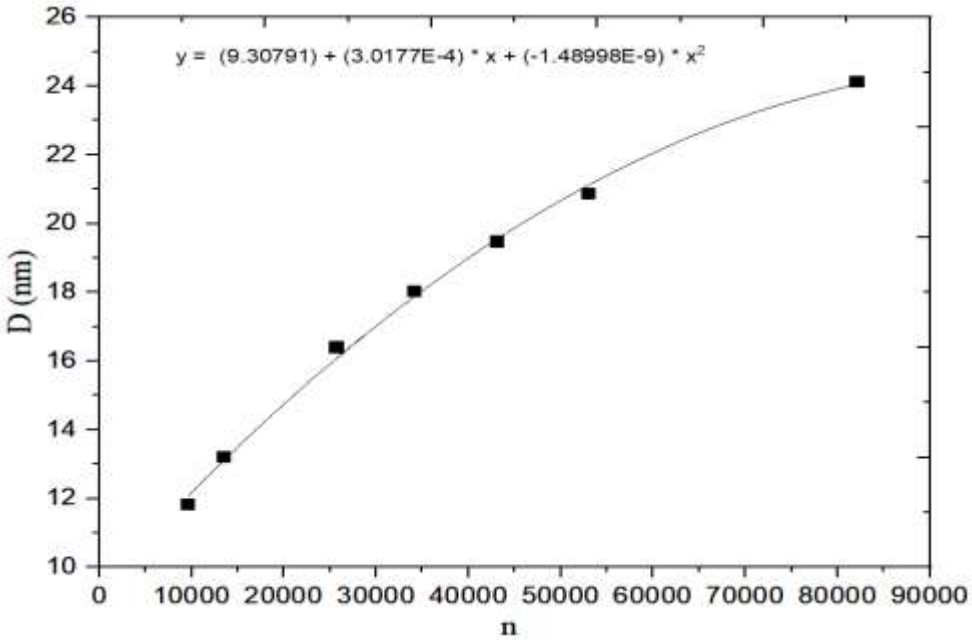

Figure 6. The relationship between crystalline size (D) and unit cell (n)

5. Conclusion

1. The Sharrer method gives direct results when calculating the crystalline size and strain without using a graph as is usual in other methods for the analysis of X-ray diffraction lines, so this method is considered fast in giving results.
2. The value of the dislocation density depends on the value of the grain size, where the dislocation density decreases with the increase in the grain size of each line of (XRD) pattern, due to the lack the width at the middle of the diffraction intensity.
3. The number of unit cells decreases when the linear dislocation density of the crystal increases, due to the increase in the volume occupied by the cells.
4. The change in the particle size values depends directly on the unit cells, as the particle size values increase with the rise in the unit cells and for each diffraction line.

Acknowledgment

I extend my thanks to the College of Education for pure science Ibn Al-Haitham, University of Baghdad for assisting in completing this work by opening private laboratories and providing scientific facilities by the staff of the Physics Department to help support the research project.

Conflict of Interest

The authors declare that they have no conflicts of interest.

Funding

None.

References

1. Dennis, C. B. Elements of X-ray Diffraction. *Addison-Wesley Publishing* **1956**, *23*, 12-23.
2. Bunaciu, A. A.; Udristioiu, E. G.; Aboul-Enein, H. Y. X-Ray Diffraction: Instrumentation and Applications. *Critical Reviews in Analytical Chemistry* **2015**, *45(4)*, 289–299. https://doi.org/10.1080/10408347.2014.949616 .
3. GalánLópez, J.; Kestens, L. A. A multivariate grain size and orientation distribution function: derivation from electron backscatter diffraction data and applications. *Journal of Applied Crystallography* **2021**, *54(1)*, 148-162. https://doi.org/10.1107/S1600576720014909 .
4. Ihsan, A. A.; Harabbi, K. H. Restriction of Particle Size and Lattice Strain through X-ray Diffraction Peak Broadening Analysis of ZnO Nanoparticles. *Advances in Physics Theories and Applications* **2015**, *49*, 34-45.
5. Rabiei, M.; Palevicius, A.; Monshi, A.; Nasiri, S.; Vilkauskas, A.; Janusas, G. Comparing methods for calculating nano crystal size of natural hydroxyapatite using X-ray diffraction. *Nanomaterials* **2020**, *10(9)*, 1-21. https://doi.org/10.3390/ma13194380 .
6. Warren, B. E. X-ray diffraction methods. *Journal of applied physics* **1941**, *12(5)*, 375-384.
7. Whittig, L. D.; Allardice, W. R. X-ray diffraction techniques. *Methods of Soil Analysis: Part 1 Physical and Mineralogical Methods* **1986**, *5(1)*, 331-362. https://doi.org/10.1063/1.1712915 .
8. Suhir, A. J.; Harbbi, K. H.; A comparative study of Williamson-Hall method and size-strain method through Xray diffraction pattern of cadmium oxide Nanoparticle. *AIP Conference Proceedings* **2020**, *2307, 1*, 1-12. https://doi.org/10.1063/5.0033762 .
9. Sami, A. M.; Harbbi, K. H. Analysis the average lattice strain in the crystal direction (hkl) in MgO nanoparticles by using modified Williamson-Hall method. *Journal of AIP Conference Proceedings* **2022**, *2394(1)*, 1-12. https://doi.org/10.1063/5.0122941 .

10. Hussein, S. K.; Harbbi, K. H. Analysis of X-ray diffraction lines profile of TiO_2 nanoparticles to determine the energy per unit volume and stress by using Halder-Wagner method. *Journal of AIP Conference Proceedings* **2022**, *2386(1)*, 1-11.
11. Yaremiy, I. P.; Bushkova, V. S.; Bushkov, N. I.; Yaremiy, S. I. X-ray Analysis of $NiCrxFe_{2}–xO_{4}$ Nanoparticles Using Debye-Scherrer, Williamson-Hall and Size-strain Plot Methods. *journal of nano- and electronic physics* **2019**, *11(4)*, 04020-1.04020-8. https://doi.org/10.21272/jnep.11%284%29.04020 .
12. Jalil, M. T.; Harbbi, K. H.; Using the Size Strain Plot Method to Specify Lattice Parameters. *Ibn Al-Haitham Journal for Pure and Applied Sciences* **2023**, *36(1)*, 123-129.
13. Obaid, M. A.; Harbbi, K. H.; Abd, A. N. Preparation and characterization of copper oxide by adding turmeric powder. *Ibn Al-Haitham Journal for Pure and Applied Sciences* **2021**, *36(1)*, 1-7. https://doi.org/10.1016/J.POLYMER.2015.07.006 .
14. Musa, K. H.; Al- Saadi, T. M. Investigating the Structural and Magnetic Properties of Nickel Oxide Nanoparticles Prepared by Precipitation Method. *Ibn Al-Haitham Journal for Pure and Applied Sciences* **2022**, *36(1)*, 94-103. http://dx.doi.org/10.30526/35.4.2872
15. Jassim, A. A.; Jassim, W. H. Preparation of Polyester/ Micro Eggshell Fillers Composite as Natural Surface Coating. *Ibn Al-Haitham Journal for Pure and Applied Sciences* **2023**, *36(1)*, 88-99.
16. Monshi, A.; Foroughi, M. R.; Monshi, M. R.Modified Scherrer equation to estimate more accurately nano-crystallite size using XRD. *World journal of nanoscience and engineering* **2012**, *2(3)*, 154-160. https://doi.org/10.4236/WJNSE.2012.23020 .
17. Bindu, P.; Thomas, S.Estimation of lattice strain in ZnO nanoparticles: X-ray peak profile analysis. *Journal of Theoretical and Applied Physics* **2014**, *8*, 123-134. https://doi.org/10.1007/S40094-014-0141-9 .
18. Abd El-Sadek, M. S; Wasly, H. S.; Batoo, K. M. X-ray peak profile analysis and optical properties of CdS nanoparticles synthesized via the hydrothermal method. *Applied Physics* **2019**, *125(283)*, 1-17.
19. Al-Jubory, A. A. Study of the effect of copper doping on the structural and optical properties of CdO.7ZnO.3S nanocrystalline thin films prepared by chemical bath deposition. *International Journal of Science and Technology* **2012**, *2(10)*, 707-712.
20. Muniz, F. T. L.; Miranda, M. R.; Morilla dos Santos, C.; Sasaki, J. M. The Scherrer equation and the dynamical theory of X-ray diffraction. *Acta Crystallographica Section A: Foundations and Advances* **2016**, *72(3)*, 385- 390. https://doi.org/10.1107/S205327331600365X .
21. Gumus, C.; Ozkendi, O. M.; Kava, H.; Ufuktep, Y. Structural and optical properties of zinc oxide thin films prepared by spray pyrolysis method. *Journal of optoelectronics and advanced materials* **2006**, *8(1)*, 299-303. https://doi.org/10.1016/j.rinp.2019.02.082 .
22. Mohammed, R. A.; Murbat, H. H.; Ahmood, S. I. Study the Effect of Cold Plasma on the Structure and Surface Properties of PbO Thin Film. *International Journal of Science and Research (IJSR)* **2017**, *69(7)*, 240-243.
23. Prabhu, Y. T.; Rao, K. V.; Kumar, V. S. S.; Kumari, B. S. X-ray analysis by Williamson-Hall and size-strain plot methods of ZnO nanoparticles with fuel variation. *World Journal of Nano Science and Engineering* **2014**, *4(1)*, 1-8. http://dx.doi.org/10.4236/wjnse.2014.41004 .
24. Gonçalves, N. S.; Carvalho, J. A.; Lima, Z. M.; Sasaki, J. M.Size–strain study of NiO nanoparticles by X-ray powder diffraction line broadening. *Materials Letters* **2012**, *72*, 36-38.
25. Parashar, M.; Shukla, V. K.; Singh, R. Metal oxides nanoparticles via sol–gel method: a review on synthesis, characterization, and applications. *Journal of Materials Science: Materials in Electronics* **2020**, *31(5)*, 3729-3749. https://doi.org/10.1007/s10854-020-02994-8 .
26. Rai, R.; Triloki, T.; Singh, B. K. X-ray diffraction line profile analysis of KBr thin films. *Applied Physics A* **2016**, *122*, 1-11. https://doi.org/10.1007/s00339-016-0293-3 .
27. Devamani, R. H. P.; Alagar, M. Synthesis and characterization of Lead (II) Phosphate Nanoparticles. *NanoTechnology* **2013**, *61*, 16922-16926. https://doi.org/10.6088/IJASER .0020101078 .
28. Abdel Abbas, S. B.; Harbbi, K. H. Elimination of the broadening in X-ray diffraction lines profile for nanoparticles by using the analysis of diffraction lines method. *Journal of AIP Conference Proceedings* **2022**, *2386(1)*, 1-12. https://doi.org/10.1063/5.0067983 .

29. Devamani, R. H. P.; Alagar, M. Synthesis and Characterisation of Copper II Hydroxide Nano Particles. *Nano Biomed Eng*. **2013**, *5(3)*, 116-120. https://doi.org/10.6088/IJASER.0020101078 .

30. Ansari, M. A.; Jahan N. Structural and Optical Properties of BaO Nanoparticles Synthesized by Facile Co-precipitation Method. *Materials Highlights Journal* **2021**, *2(2)*, 23–28. https://doi.org/10.2991/MATHI.K.210226.001 .